Acta Geophysica
https://doi.org/10.1007/s11600-022-00965-7

RESEARCH ARTICLE - HYDROLOGY

Discharge estimation and rating curve derivation, using satellite geometry data and isovel contours at Karun River, Iran

Hossein Farnoush[1] · **Mahmoud F. Maghrebi**[1]

Received: 9 March 2022 / Accepted: 3 November 2022

Abstract

Determining discharge and stage–discharge curves in fluvial environments without hydrometric gauges is a critical challenge in hydrologic studies and river hydraulics. This issue will be more evident in managing flood hazards in the rivers of arid areas without flow measurement gauges, where the reaction time is the critical factor. Researchers and designers have always tried to access simpler, cheaper methods to estimate discharge and rating curves. This research aims to facilitate the determination of the discharge and stage–discharge relationship by applying remote sensing techniques and the concept of isovel contours. For this purpose, the geometry of the river cross section is determined using remotely sensed data from the images of the Sentinel-1 and two satellites, and then discharge passed through the cross section is estimated by the single point velocity measurement method. The observed data were collected from the Mollasani station in Karun River, Iran, to confirm this method. The obtained discharges and stage–discharge relationship curves are used to evaluate the accuracy of the proposed methodology. Statistical analyses showed that the mean value of the normalized percentage error and mean absolute percentage error (MAPE) calculated based on the difference between the estimated and observed discharges are limited to 6.3 and 8.36%, respectively. Also, the stage–discharge curves in these studies were estimated with a maximum MAPE of 9.5%, which is considered a good initial approximation considering the minimum required data.

Keywords Discharge estimation · Stage–discharge · Isovel contours · Remote sensing satellite · Single point velocity measurement method (SPM) · Karun river

List of symbols

A	Cross-sectional area of flow
B	Open-channel width
c, c_1, c_2, c_2	Proportionality constant
C	Normalized velocity
$\mathrm{d}u$	Differential velocity deviation between an element of the boundary and an arbitrary point in the flow field
$f()$	A function of
H	Water depth along y-axis at a cross section
k_s	Equivalent Nikuradse sand roughness
m	Constant; exponent of power formula
P	Wetted perimeter
Q	Discharge
Q_0	Observed discharge
Q_e	Estimated discharge
r	Position vector of arbitrary point in field
r	Subscripts, represents the referenced value
e	Subscripts, represents the estimated value
u_m	Measured velocity component in the streamwise direction
u	Local velocity
U	Average cross-sectional velocity
u_*	Boundary shear velocity
$\mathrm{d}u_{\mathrm{SPM}}$	Effect of $\mathrm{d}\mathbf{s}$ from the wetted perimeter on the velocity at an arbitrary point with the coordinates of (y, z)
n	Manning roughness equivalent
y	Normal distance from the wall (left bank)
θ	Angle between the positional vector $\mathbf{r}$ and the boundary element vector $\mathrm{d}\mathbf{s}$
$T_{\max}$	Maximum width of the water surface
τ_0	Boundary shear stress
u_{SPM}	Local point velocity

Edited by Dr. Michael Nones (CO-EDITOR-IN-CHIEF).

✉ Mahmoud F. Maghrebi
maghrebi@um.ac.ir

[1] Department of Civil Engineering, Ferdowsi University of Mashhad, Mashhad 91775-1111, Iran

(y, z)	An arbitrary position in the channel section
σ°	Output radar backscatter bands

Introduction

River discharge measurements are required for flood control, water resources management, climate change, and hydrology studies. In recent decades, hydrology and hydraulic engineers have determined river discharges using remotely sensed data. In general, methods to measure discharge can be classified into three groups. The first group is based on hydraulic flow parameters such as the wet channel width, wetted perimeter, river inundation geometry, water level, and channel slope, which the Manning formula (or modified manning formula) can calculate discharge. The second group relies on hydraulic and hydrologic models, and finally, the third group uses a combination of hydraulic models with obtained data such as velocity.

Satellite sensors are powerful tools for observing hydrological phenomena and river changes due to their global coverage, continuous monitoring, and long historical archives of observations. The geometric characteristics of flow cross section in rivers can be obtained by optical satellite images such as Landsat, SPOT, IKONOS, MODIS, and Quick Bird and some SAR images such as Radarsat-1/2, Envisat, JERS-1, and ERS-1/2.

The choice of the satellite data to be used in a specific river monitoring application depends on many factors such as the river size (length and width), the spatial resolution required, the physical properties of the objects to be observed, the duration of the observation period and the frequency with which changes need to be tracked (Gilvear and Bryant 2016).

Many researchers have estimated discharge in natural rivers using hydraulic and hydrologic models with remote sensing instruments. Smith et al. (1995, 1996) indicated that ERS-1 synthetic aperture radar images (SAR) and simultaneous ground measurements of discharge were useful in estimating discharge in braided rivers in the Arctic region (Smith et al. 1995, 1996). The ERS-1 sensor has a spatial resolution of 25 m. By defining the effective width parameter, which is the result of the water surface area obtained from the SAR satellite images in the braided area divided by the reach length, and establishing a correlation with the power relationship between the effective width and discharge and comparing it with observed discharges, they developed a method for estimated discharge. Synthetic values of effective width and discharge generated from a flow weaving cellular automata model show a similar power law correlation.

Al-Khudhairy et al. (2002) showed that utilizing a statistical relationship, the effective wet ditch width acquired from multi-temporal Landsat TM pictures and simultaneous ground-based measurements of water levels may be used to estimate the water surface in three European wetlands. These relationships can then estimate historical ditchwater levels and monitor contemporary ditchwater levels in the wetlands. Coe and Birkett (2004) estimated lake height using satellite altimetry in ungauged locations in experiments on the Lake Chad Basin. For this purpose, in situ altimetric stage measurements from the TOPEX/Poseidon satellite (T/P) with ground-based information were used. Via simple linear correlation methods, the stage measurements successfully estimate the height of the permanent waters of the lake. For 75 percent of the observed times, the results demonstrated a 20 percent accuracy. Due to seasonal water flows into the lake, other times were less accurate. Xu et al. (2004) used in situ measurements and Quickbird-2 images to calculate the Yangtze River's discharge by creating width-stage and stage–discharge relationships. Bjerklie et al. (2005) estimated the river discharge by applying single C-band AirSAR satellite images and a modified Manning equation. The channel widths of the wet channel were collected from 26 aerial and digital orthophotos and 41 SAR pictures for their research. They obtained the slope of the channel using DEM data. Surface velocity was calculated from AirSAR. The error associated with the estimated discharge was obtained at 10% using a developed model.

Maghrebi (2006) has estimated the discharge in rectangular channels using the single point velocity Measurement method (SPM). This study describes the fluid flow system as an equivalent electromagnetic system. A successful application of the Biot–Savart law in hydraulics is presented. The similarity between the magnetic field around a current wire and isovel lines in a channel cross section is used to derive velocity patterns in an open or closed channel. The precision of his model was confirmed by data collected from the Severn River in the United Kingdom.

Furthermore, this method can estimate discharge faster and at a lesser cost. Smith and Pavelsky (2008) estimated the discharge of the Lena River in Siberia using 65 cloud-free MODIS images by acquired effective width. Results have revealed that the effective measured width had a mean absolute error of less than 25% with a correlation coefficient of 0.81. To forecast downstream discharge conditions, the mean observed and calculated velocities (using satellite images) were 0.97 and 1.01 m/s, respectively. Moreover, one of the most critical problems of optical pictures is their inability to provide images in the presence of the cloud. SAR remote sensing by penetrating the cloud cover can overcome this limitation. Therefore, this technique will be more effective in small basins.

Schumann et al. (2009) used radar altimeters to measure the water level and its changes in large rivers, which they introduced as rivers that have satellite data with a land resolution of more than 100 m. Tarpanelli et al. (2013) estimated

river discharge variations using moderate resolution imaging spectroradiometer (MODIS) data in ungauged basins. Their study has shown that MODIS data can give more accurate discharge estimations for medium-sized basins (less than 10,000 km^2), characterized by high temporal variability. The capability of MODIS to estimate the mean flow velocity could be efficiently employed for rating curve development at ungauged river sites. Gleason et al. (2014) estimated the discharge using Landsat TM satellite images of the river width and the log-linear relationships at a hydraulic station for some types of river reaches. Paris et al. (2016) determined rating curves by applying satellite altimetry to a poorly gauged basin. They analyzed the Amazon Basin using nearly one thousand series obtained from ENVISAT and Jason-2 altimetry for more than 100 tributaries.

In most of the previous studies, by defining parameters such as the effective width of the wet channel or planimetric surface of the wet channel obtained from satellite data and prescribing the correlation relationship with the observed discharges in the existing stations by fitting the regression relationship, discharge estimation has been achieved. However, in this study, by using the velocity distribution pattern (Isovel), the geometric characteristics of the river and the surface velocity of the flow, which is much easier to extract, and relying on the hydrodynamics of the flow, the discharge is estimated independently of the data available in the hydrometric stations. The primary goal of this work is to calculate the isovel contours at the cross section of flow using a model developed by Maghrebi (2006) and remotely sensed data from the Sentinel-1/2 satellites to estimate the stage–discharge curve in the Karun River in Iran. For the first time, this paper uses the surface water velocity to estimate discharge and rating curve based on Maghrebi's method.

Study area

The Karun River is the longest and the most important permanent river located southwest of Iran (See Fig. 1). The basin area of this river is about 77,340 km^2. There are several hydrometry stations located along this river. Mollasani station is located in the geographical position with the coordinates of 31°35′N and 48°53′E. The average and maximum discharge of the Karun River at Mollasani station are 575 and 3300 m^3/s, respectively, and the longitudinal slope at this station is estimated to be about 0.0001. In this station, only the water surface stage is read via gauge height (twice on normal days and every half hour during floods). Twice a year, depth information is obtained from the boat and the ruler, and the propeller collects velocity information at various depths. Then, the rating curve is extracted and obtained in other cases, especially the daily discharge measurement, through the stage reading and the rating curve. Water surface velocity, stage, and discharge in 2 different stages of river flow and cross-sectional geometry are taken from ground measurements to validate the performance of the proposed method (Fig. 2).

Materials and methods

Each material on the ground surface has its spectral signature due to the reflection, absorption, and transmission of the radiation received at different wavelengths (Gilvear and Bryant 2016). Water has a particular spectral behavior that is generally in contrast with other elements that surround it. It has a higher transmissivity coefficient in the visible

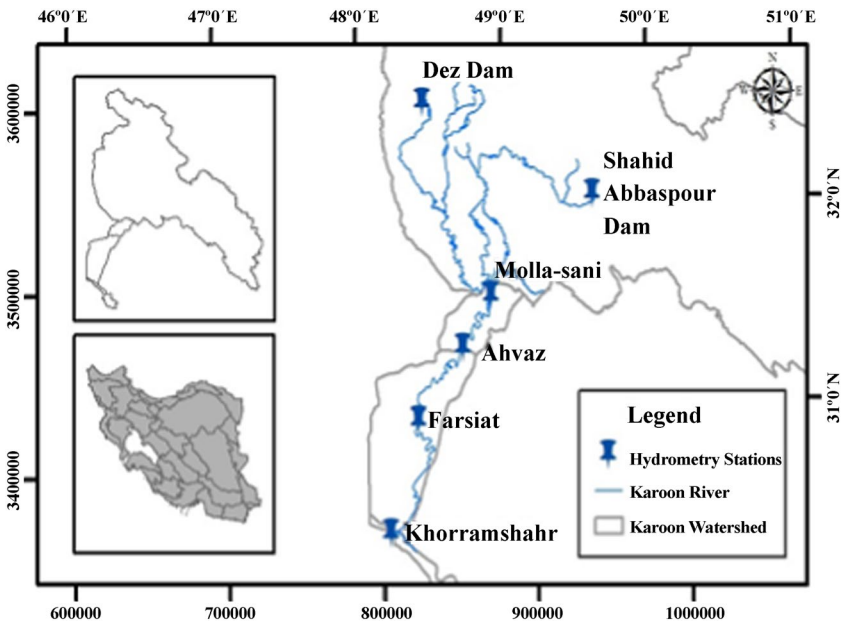

Fig. 1 The geographical location of the Mollasani station

wavelengths than in the NIR and SWIR wavelengths. Indeed, clear water absorbs in the near-infrared (NIR) and shortwave infrared (SWIR) wavelengths while reflecting in the visible wavelength (VIS) when suspended particles are present in the water, like in rivers, the reflectance increases for longer wavelengths (NIR). The clear water reflectance spectrum peaks in the green wavelength band (0.50–0.56 m) and decreases against increasing wavelengths, reaching a reflectance close to zero in the near-infrared (NIR) region (0.75–1.4 m). The turbid water reflectance spectrum exhibits higher values than clear water in the near-infrared region and approaches zero at longer wavelengths. This is due to the concentration of solutes, sediments, and organic matter, whose presence reinforces the reflection in the near-infrared band. Typically, the water of rivers contains solid particles and appears not clear. In the case of shallow water, the turbidity of the surface layer can be particularly high. Furthermore, in the case of shallow transparent water, the spectral signature can be influenced by the reflectance of the bed (Cavallo et al. 2021b).

For monitoring river hydro-processes or small-scale analysis in medium rivers width in the range of 20–200 m, very high-resolution satellite images (e.g., Geo Eye, World View, Quick Bird, and Planet) are suitable (Gilvear and Bryant 2016). However, acquiring very high spatial-resolution images of large areas in most cases is still too expensive. A limited number of high-resolution images is freely available (e.g., on the Google Earth Pro Platform), but the temporal resolution is relatively poor. As of now, freely available data with adequate temporal resolution (a few days) are available only at moderate spatial resolutions (10–30 m) (Cavallo et al. 2021a).

Sentinel-1/2 belongs to this group: they provide multispectral images with variable resolutions (10, 20, 30, 60 m) according to the band, with short revisit times, in the range of 5–9 days. The minimum width of the river that can be monitored is equal to three image pixels. Therefore, Landsat and Sentinel-2 data can be used for rivers wider than 90 and 30 m, respectively (Jiang et al. 2014). These data offer the opportunity to perform analysis at various spatial scales. The needed spatial resolution depends on the dimension of the target: in the case of rivers, the relevant dimension is the width and depth (Gilvear and Bryant 2016). The time resolution depends on the speed of evolution of the observed process (Boothroyd et al. 2021).

Sentinel-1/2 (S1 and S2) missions are part of the Copernicus Earth Observation program led by the European Commission and operated by the European Space Agency (ESA). One of the weaknesses of using optical images is the presence of cloud cover before and at the same time as the flood occurs. These clouds prevent electromagnetic waves from reaching the sensors from the earth's surface. Therefore, using radar images (SAR) is suitable for the presence of cloud cover because radar images in all weather conditions and throughout the day and night provide us with accurate information about the requirements of the Earth surface with an appropriate spatial resolution (Matgen et al. 2007). However, the algorithms that derive the required data from SAR images have a complex design compared to optical sensors.

Sentinel-1 (S1) mission performs radar imaging (Synthetic Aperture Radar, SAR) and can monitor phenomena and effects throughout the day and night regardless of weather and cloud cover conditions. This satellite captures images with an acceptable resolution of up to 5 m and coverage of 400 km in the microwave and C-band wavelength ranges and four different modes with a virtual aperture radar. Sentinel-1 satellite combines two satellites, A1 and B1, which provide images with a spatial resolution of 20 m in the C band with VH and VV polarization. The polarity of its orbit and the dual polarization capability of this satellite have caused fast data transmission from the satellite to ground stations. S1A and -B, the next generation of C-band (center frequency 5.405 GHz) radar missions, were launched on 3 April 2014 and 25 April 2016, respectively. The revisit

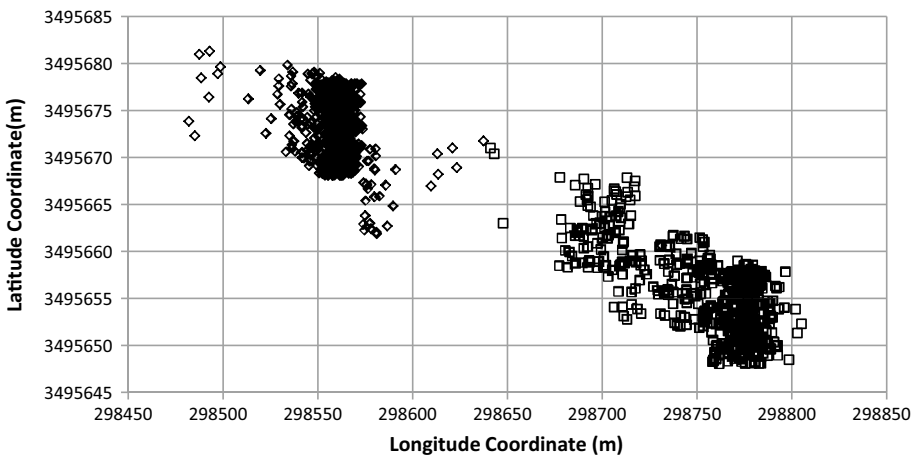

Fig. 2 Spatial position of the centroid of water shoreline pixels along the Karun River cross section at the Mollasani station (Sentinel 1/2 images (2014–2020))

time of a single satellite is 12 days, whereas the two-satellite constellation provides a revisit time of 6 days.

Sentinel-2 (S2) mission, a European polar-orbiting, high-resolution optical imaging satellite, is used for earth observation and monitoring phenomena such as water, soil, and vegetation. This satellite's systematic global coverage of land surfaces is from 56 °S to 84 °N, coastal waters, and all of the Mediterranean Sea. It has a lifespan of 7 years. (S2) mission consists of two satellites (A and B), carrying on board the Multispectral Instrument (MSI), which has provided moderate-resolution imagery since June 2015 (Sentinel-2A) and March 2017 (Sentinel-2B).

The Sentinel-2 satellites have different spatial resolutions of 10, 20, and 60 m, with 13 spectral bands in the visible/near-infrared (VNIR) and short wave infrared spectral range (SWIR): 443–2190 nm (including three bands for atmospheric corrections). The MSI sensor of this satellite uses 13 different bands in the visible and infrared range, the blue band (B2), green (B3), red (B4) and near-infrared (B8) with a resolution of 10 m, near infrared bands (B5), (B6), (B7), (B8A) and short-wave infrared (B11, B12) with 20 m resolution and finally, its coastal aerosol band (B1), short wave infrared (B9) and (B10) have a resolution of 60 m.

This study grouped the varied land cover types into three classes: open water, the mosaic of water, mud and vegetation, and bare soil land. Classification of these three classes was obtained through a rule-based method that combined the SWI, NDWI, and MNDWI indices.

Classification method

In this study, the Sentinel-2 images were processed to derive the Normalized (or Modified Normalized) Difference Water Index (NDWI and MNDWI), validating the classification method via higher-resolution Sentinel-1 SAR images.

The differences in spectral signatures are typically exploited for the automatic land cover classification, defining appropriate multispectral indices. To obtain the Normal Difference Water Index (NDWI), a combination of bands from near-infrared bands to investigate and separate water (lakes and internal wetlands from seas) is used. For instance, the widely used Normalized Difference Water Index (NDWI) is defined as flows (McFeeters 1996):

$$\mathrm{NDWI} = \frac{\rho_{\mathrm{green}} - \rho_{\mathrm{NIR}}}{\rho_{\mathrm{green}} + \rho_{\mathrm{NIR}}}, \tag{1}$$

where ρ_{green} and ρ_{NIR} are the reflectivity in the green and NIR bands, it can be argued from the spectra that positive values of NDWI will characterize areas covered with clean water. On the contrary, it is expected that the surfaces surrounded by turbid waters will manifest almost null values of NDWI.

Xu et al. (2006) used the Modified Normalized Difference Water Index (MNDWI), extracted from the combination of satellite-derived data, the B3 green band, and the B11 shortwave infrared (SWIR) band dataset, to discriminate open water areas in study regions:

$$\mathrm{MNDWI} = \frac{\rho_{\mathrm{green}} - \rho_{\mathrm{SWIR}}}{\rho_{\mathrm{green}} + \rho_{\mathrm{SWIR}}}. \tag{2}$$

In contrast, clean and turbid water will be characterized by positive values of MNDWI, which uses the short-wavelength infrared ρ_{SWIR} (1.4–3 μm) in place of the NIR reflectivity. SWI index used to exploit open water surface from bare soil land and for Sentinel-1 SAR images is used based on point detection and statistical analysis. The algorithm's derivation of the SWI index from S1A- SAR images has more complexity. Five basic steps are used to extract this index: First, S1A images were allocated orbit files. Second, S1A images were radiometrically calibrated to output radar backscatter bands (σ°). Third, radar backscatter bands were orthorectified using the Range Doppler Terrain Correction algorithm with SRTM DEM and spatial resolution of 1 S. Fourth, the backscattering coefficient (in dB) was acquired from the orthorectified radar backscatter band by the Eq. $10 \times \log_{10}(\sigma^{\circ})$. Fifth, a median filter with a window size of 5×5 pixels was utilized to remove speckle noises (Tian et al. 2017). The threshold values were confirmed as $-$ 23 dB and $-$ 17 dB based on VH and VV imagery, respectively. For a single band, a pixel was classified as water if its value was less than $-$ 23 dB in VH imagery or $-$ 17 dB in VV imagery, respectively. Due to the filtration steps, polarization and extraction of the SWI index were done through coding in the Google Earth Engine plugin, and further explanations were avoided.

Since on the one hand, the subject of this study is to detect the contact point of water with land at the level of flooding along a section of the river, and not necessarily to calculate the planimetric surface of the wet channel area, and on the other hand, in the NDWI index and according to the use of Sentinel-2 images, every two parameters used (b_3, b_8) have a spatial resolution of 10 m, so NDWI was used here to achieve more accuracy.

The width of the wet channel is given by the envelope of the width of the cross section in correspondence with the free surface. This is strictly dependent on the water level according to a relationship that expresses the geometry of the cross section.

The cross-sectional geometry was determined using the Sentinel-1 and -2 satellite images on various dates. First, based on the available images, the intersection of the water surface with the land was determined. For this purpose, the water area in each image is determined by using S1-SAR and S2 images and basic processing and corrections, including

radiometric calibration, atmospheric and altitude corrections, and the NDWI. These images show areas of water in a dark color, while natural ground sends a lot of energy from the radar waves to the sensor due to the roughness of the surface. This situation causes a sharp difference between the water and soil environment and makes water and soil areas be identified. In this study and to improve the result, the images of both Sentinel 1 satellite with a spatial resolution of 20 m and Sentinel-2 with a spatial resolution of 10 m were used simultaneously, and the coordinates of the pixel center between land and water (intersection of land and water) were extracted. Then, based on the coordinates of these points using available DEM in the area, a set of points was obtained showing the intersection point of water and land on different dates. From the analysis of this cloud data, the river cross section was determined. For this purpose, the Google Earth Engine plugin was efficiently used in several programming lines. One of the features of this plugin is the ability to use all available images from one area taken by different satellites with different spatial resolutions.

Cross-sectional geometry can be estimated using intersection coordinates of the cross section and the water surface. Then, the water surface width variations at different times and the stage of the right and left banks are extracted using the 25 m spatial resolution digital elevation model (DEM). The average height in each image is used to check the observed data due to the constant water level on the right and left banks. The bottom elevation of the river is also determined using its DEM. Table 1 shows some of these data obtained at specific times from the Karun River at the Mollasani station. Figure 3 compares the actual cross section with the remotely sensed data. Typically, the determination of the cross-section geometry below a specified level is impossible with visible images, as the water level does not fall below this level in a permanent river. Therefore, the geometry data of the cross section should be completed using other auxiliary data such as DEM. The equivalent rectangle cross section has been used to complete the cross section in Fig. 3.

Using remotely sensed data can accurately determine the shape of river cross sections, especially permanent ones. After recognizing the geometry of the cross section, discharges passed through the cross section can be estimated by the single point velocity measurement method (SPM), which is based on isovel contours (Maghrebi and Ball 2006).

The essential ability of the present method is that discharge can be calculated using just a single point of velocity measurement. At the Mollasani station, velocity was measured at four different observed points (See Fig. 4). Discharge can be calculated based on each observed velocity measurement at P1, P2, P3, and P4. P1, P2, and P3 are near the water surface at $h \approx 0.98H$. However, P4 is located at $h \approx 0.8H$. It should be noted that the estimated discharge based on each point of velocity measurement is different from the others.

According to Fig. 4, the maximum width of the water surface ($T_{\max}$) at the Mollasani station is 265 m. The velocity magnitude (u_m) has been measured at two water depths: $H = 4.05$ m and $H = 6.07$ m. The observed discharges (Q_0) and the cross-sectional areas (A) corresponding

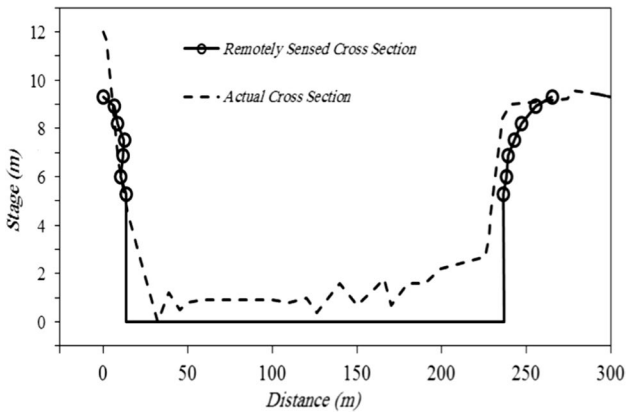

Fig. 3 The geometry of the Karun River cross section at the Mollasani station

Table 1 Some data obtained from Sentinel images at the Mollasani station

Frame no	Date	Left bank coordinates		Right bank coordinates		Width of the free surface, T(m)
		x(m)	y(m)	x(m)	y(m)	
1	19/03/2016	298,565.3	3,495,724.8	298,794.8	3,495,665.0	237.2
2	31/03/2016	298,564.8	3,495,724.8	298,794.7	3,495,665.0	237.5
3	08/04/2016	298,565.1	3,495,725.1	298,795.0	3,495,669.6	236.5
4	18/04/2016	298,554.9	3,495,725.4	298,875.0	3,495,664.5	237.92
5	28/04/2016	298,554.9	3,495,725.3	298,805.3	3,495,664.9	257.6
6	08/05/2016	298,564.6	3,495,734.8	298,805.0	3,495,663.8	250.6
7	18/05/2016	298,565.0	3,495,725.1	298,794.6	3,495,665.2	237.3
…	…	…	…	…	…	…
534	10/12/2020	298,568.57	3,495,668.44	298,758.57	3,495,648.44	191.05

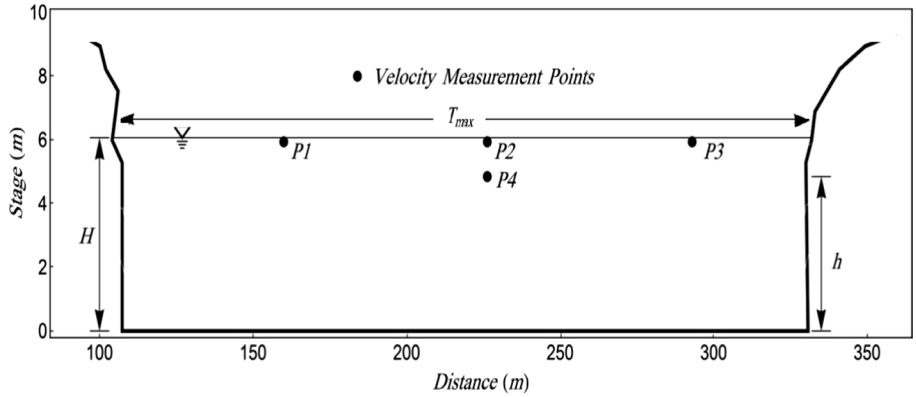

Fig. 4 Schematic view of measured velocity points at the Mollasani station

Table 2 Specifications of the measurements at $H = 4.05$ m

Point of velocity measurement	$\approx y/T_{max}$	$\approx h/H$	u_m (m/s)	Obs. discharge-Q_0 (m^3/s)
P1	0.25	0.98	1.57	953
P2	0.5	0.98	1.77	
P3	0.75	0.98	1.48	
P4	0.5	0.8	1.78	

Table 3 Specifications of the measurements at $H = 6.07$ m

Point of velocity measurement	$\approx y/T_{max}$	$\approx h/H$	u_m (m/s)	Obs. discharge-Q_0 (m^3/s)
P1	0.25	0.98	1.86	1859
P2	0.5	0.98	1.99	
P3	0.75	0.98	1.81	
P4	0.5	0.8	2.01	

to $H = 4.05$ m and $H = 6.07$ m are 953 m^3/s, 1859 m^3/s, 904.4 m^2, and 1354.4 m^2, respectively.

Tables 2 and 3 illustrate more data on each point of velocity measurement at two water depths of $H = 4.05$ and 6.07 m, respectively. In Tables 2 and 3, y/T_{max} is measured from the left bank.

Principles of the single point velocity measurement method (SPM)

Maghrebi (2003, 2006) introduced the single-point velocity measurement method. The main idea originates from this method's boundary effect on the cross-sectional velocity. It is hypothesized that the boundary of a river moves with the velocity of river flow. Therefore, no velocity distribution will be formed at the river section. However, the velocity distribution in natural rivers will be formed with zero values on the boundary and larger values further away from the boundaries. The boundary effects are simulated with the electromagnetic field generated by an electric current in a wire at a 2D plane. The Biot–Savart law is used to formulate the problem (Maghrebi 2006).

Figure 5 shows a schematic sketch of the Mollasani cross section, covered with triangular meshes. The centroid of each triangular element is where the boundary effects are calculated. The number of meshes has been increased along the boundary and the water surface to increase the method's accuracy.

Chen (1991) showed the power-law velocity distribution of the steady uniform turbulent flow in an open channel as:

$$\frac{u}{u_*} = c\left(\frac{y}{k_s}\right)^{1/m}, \tag{3}$$

where u is the local velocity at normal distance y from the walls; $u_* = \sqrt{\tau_0/\rho}$ is the boundary shear velocity, where τ_0 is the boundary shear stress and ρ is the mass density of fluid; k_s is the equivalent Nikuradse sand roughness height, c is a coefficient that varies with the global Reynolds number for hydraulically smooth flows or with global relative roughness for fully rough flow, and the exponent m usually ranges between 4 and 12 depending on the intensity of turbulence (Yen 2002). However, a value of 7 fitted well with many experimental measurements of turbulent velocity files for smooth boundaries (Chen 1991).

The wetted perimeter of the cross section is divided into infinitesimal elements d$\mathbf{s}$, as shown in Fig. 5. The effect of d$\mathbf{s}$ from the wetted perimeter on the velocity at an arbitrary point with the coordinates of (y, z) is $\mathbf{du}_{SPM,}$ which can be calculated using the following vector equation:

$$\mathbf{du}_{SPM} = f(\mathbf{r}) \times c_1 \cdot \mathbf{ds}. \tag{4}$$

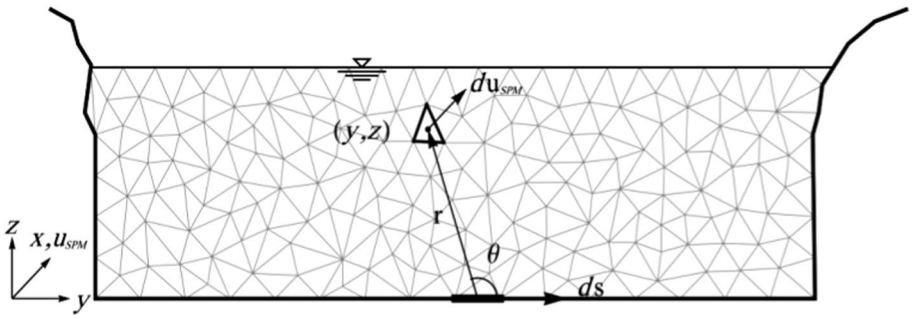

Fig. 5 Illustrative geometry for boundary effect on the velocity of an arbitrary point with coordinates (y, z) at the Mollasani station

As a result, the total effects of the boundary on each element can be integrated as follows:

$$u_{\mathrm{SPM}}(y,z) = \int_{\text{boundary}} c_1.f(r)\cdot \sin\theta \cdot \mathrm{d}s, \tag{5}$$

where c_1 is a constant which depends on the boundary shear stress, turbulent intensity, and relative roughness, θ is the angle between the positional vector **r** and the boundary element vector d**s**, and $f(r)$ is the dominant velocity function in terms of r, knowing as a power-law relationship which is commonly used to fit velocity profiles in the open channels Eq. 3 can be rewritten as:

$$f(r) = u_*\left(c_2 \cdot r^{1/m}\right), \tag{6}$$

where c_2 is related to the boundary roughness and nature of the flow. Replacing *f(r)* from Eq. 6 into Eq. 5, the local point velocity at an arbitrary position in the channel section coordinates (y, z) in Fig. 5, u_{SPM} *(y, z)*, is obtained as:

$$u_{\mathrm{SPM}}(y,z) = \int_{\text{boundary}} c_1.c_2\cdot u_*\left(r^{1/m}\right)\sin\theta\cdot \mathrm{d}s. \tag{7}$$

By considering the value of $c_1\, c_2\, u_*$ equal to c_3 and $m=7$, Eq. 7 can be rewritten as:

$$u_{\mathrm{SPM}}(y,z) = \int_{\text{boundary}} c_3\cdot\left(r^{1/7}\right)\sin\theta\cdot \mathrm{d}s. \tag{8}$$

Since the boundary roughness of the wetted perimeter of the river is assumed to be uniform, the value of c_3 is considered equal to one. The value produced from Eq. 8 has no practical significance; nonetheless, its normalized value is crucial in the single point velocity measurement method (SPM) approach. The following Equation can be used to calculate the mean cross-sectional U_{SPM}:

$$U_{\mathrm{SPM}} = \frac{\int_A u_{\mathrm{SPM}}(y,z)\cdot \mathrm{d}A}{A}, \tag{9}$$

where dA is the area of each triangular mesh and A is the total flow area. The normalized velocity C at (y, z) is obtained as follows:

$$C = \frac{u_{\mathrm{SPM}}(y,z)}{U_{\mathrm{SPM}}}. \tag{10}$$

The mean cross-sectional velocity can be calculated by measuring the local velocity u_m at any arbitrary position with the associated value of C:

$$U = \frac{u_m}{C}, \tag{11}$$

where in the above equations, u_{SPM}, $U_{\mathrm{SPM,}}$ and C are the computed quantities, and u_m is the measured one. Figure 6 shows the sensitivity of the calculated C values to the grid numbers corresponding to different velocity measurement points shown in Fig. 5. From this figure, it can be observed that when the number of the grids is increased to about 500, a minimal variation in the C value occurs, which means that the results will remain practically unchanged for larger grid numbers. A finer mesh with a total number of about 1860 has been implemented in the current computations.

Results of discharge estimation

In the first step, it is necessary to calculate the isovel contours at $H=4.05$ and 6.07 m to estimate the discharge based on the *single point velocity measurement method* (SPM). Figure 7 shows the normalized isovel contours for both levels. At this stage, the value of C can be extracted at the measured points. Then, according to Eq. 11, the average flow velocity passing through each cross section can be calculated based on the corresponding values of C and u_m.

Tables 4 and 5 show the values of parameters: normalized isovel contour *(C),* the measured velocity at the observed point *(u_m),* average cross-sectional velocity *(U)*, which is obtained by Eq. 11, total cross-sectional area *(A)* and estimated discharge *(Q_e)* at $H=4.05$ and 6.07 m, respectively. The results indicate the estimated discharges based on P1, P2, P3, and P4. Some estimated discharges are higher than

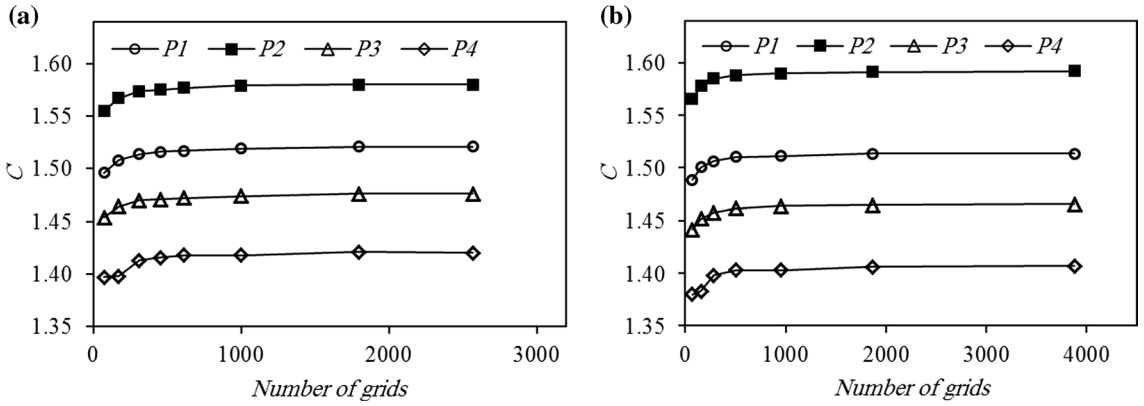

Fig. 6 Variation of the value of C with the different number of grids **a** $H=4.05$ and **b** $H=6.07$

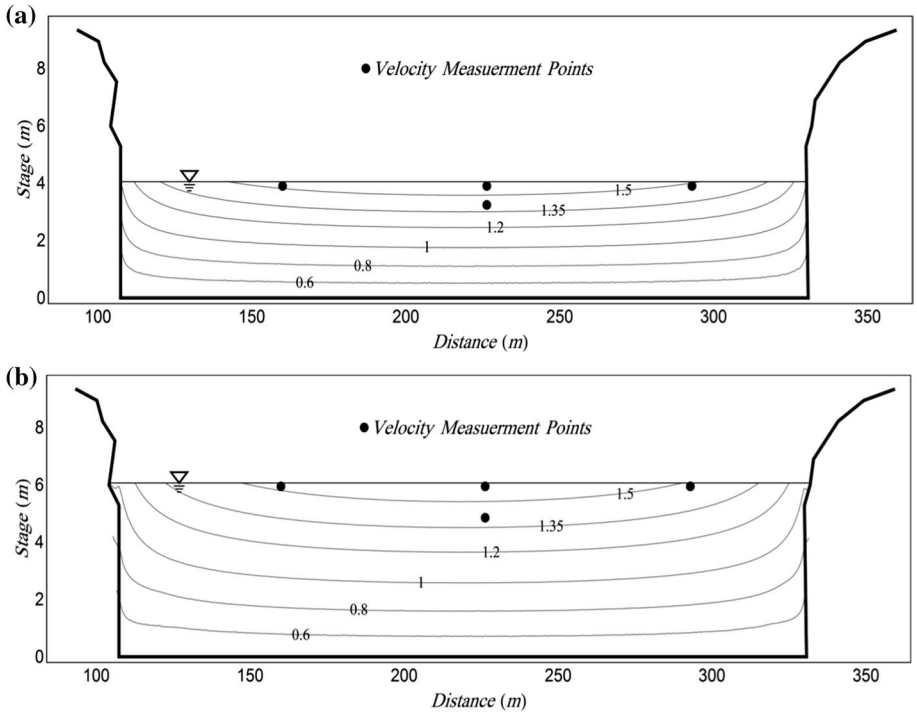

Fig. 7 The model obtained normalized isovel contours (C) at different water levels **a** $H=4.05$ m and **b** $H=6.07$ m

the observed ones, and some are lower than others. To better understand the accuracy of the proposed method, statistical analysis of estimated and observed data is necessary.

Figures 8a and b show the estimated and observed discharges based on different observed points at $H=4.05$ and 6.07 m, respectively. The estimated discharges by the *single point velocity measurement method* (SPM) based on two points of P1 and P3 are more significant than the observed discharge. Two other estimated discharges based on P2 and P4 are less than the observed discharge in Fig. 8a. Figure 8b indicates that the values of the estimated discharges based on P1 to P3 obtained from the proposed methodology are underestimated. However, the estimated discharge based on point P4 is larger than the observed one. This implies that an estimation based on the average discharge obtained from all observed data points will have a lower error percentage.

Table 4 Discharge estimation based on different observed points at $H=4.05$ m

Point of velocity measurement	u_m (m/s)	C	U (m/s)	A (m^2)	Q_e (m^3/s)
P1	1.57	1.52	1.03	904.4	933.6
P2	1.77	1.58	1.12	904.4	1013.2
P3	1.48	1.48	1.00	904.4	906.9
P4	1.78	1.42	1.25	904.4	1132.9

Table 5 Discharge estimation based on different observed points at $H = 6.07$ m

Point of velocity measurement	u_m (m/s)	C	U (m/s)	A (m^2)	Q_e (m^3/s)
P1	1.86	1.51	1.23	1354.4	1664.6
P2	1.99	1.59	1.25	1354.4	1694.2
P3	1.81	1.47	1.24	1354.4	1673.8
P4	2.01	1.41	1.43	1354.4	1936.3

Statistical analysis can evaluate the efficiency of the proposed methodology in discharge estimation. Among the standard statistical measures, the normalized percentage of error (NPE) can be defined as follows:

$$\mathrm{NPE}(\%) = \frac{Q_o - Q_e}{Q_o} \times 100, \tag{12}$$

where Q_e is the estimated discharge, and Q_o is the observed discharge. Figure 9a and b, the normalized percentage of error calculated based on Eq. 12, are shown at two water depths, $H = 4.05$, and 6.07 m, respectively. The maximum value of NPE (%) is limited to -19% in Fig. 9a. If the average discharge is calculated based on all the observed points, then the NPE (%) value will be about 4.6%. Figure 9b shows the corresponding results to Fig. 9a for the higher water depth. The estimated discharges by the *single point velocity measurement method* (SPM) based on points P1 to P3 are larger than the observed discharge, and the last one based on P4 is less than the observed discharge. The maximum absolute percentage of error is limited to 10.5%. The average discharge error based on all observed points is also limited to 6.3%.

To examine the performance of the proposed method, the statistical measure of the mean absolute percentage error (MAPE) calculated based on the estimated discharge Q_e, and the observed discharge Q_o is given as follows:

$$\mathrm{MAPE}(\%) = \frac{100}{N}\sum_{i=1}^{N}\left|\frac{(Q_o)_i - (Q_e)_i}{(Q_o)_i}\right|. \tag{13}$$

According to Tables 4 and 5, the mean absolute percentage error (MAPE) for discharge estimation at two different water depths, H = 4.05 m, and H = 6.07 m, is 8.01% and 8.36%, respectively.

Estimation of the stage–discharge curve

Using the concept of isovel contours and the single point velocity measurement method (SPM), Maghrebi and Ahmadi (2017) presented a relationship in which the stage–discharge estimation can be easily performed using the discharge data at the selected level.

Based on this proposed relationship, it is possible to estimate the rating curve for the present asymmetric compound section using the following Equation for each water level only based on the existence of a reference point of the discharge and stage, respectively:

$$Q_e = Q_r\left(\frac{A_e}{A_r}\right)^{0.972}\left(\frac{P_e}{P_r}\right)^{-1.27}\left(\frac{(P_t)_e}{(P_t)_r}\right)^{0.83}\left(\frac{(U_{SPM})_e}{(U_{SPMs})_r}\right)^{1}\left(\frac{n_e}{n_r}\right)^{-1}, \tag{14}$$

where the subscripts r and e represent the referenced and estimated values, respectively. Other variables include flow cross-sectional area (A), wetted perimeter (P), total perimeter (P_t), and Manning roughness equivalent (n). The values of parameters A, P, P_t, n, and U_{SPM} can be calculated at all

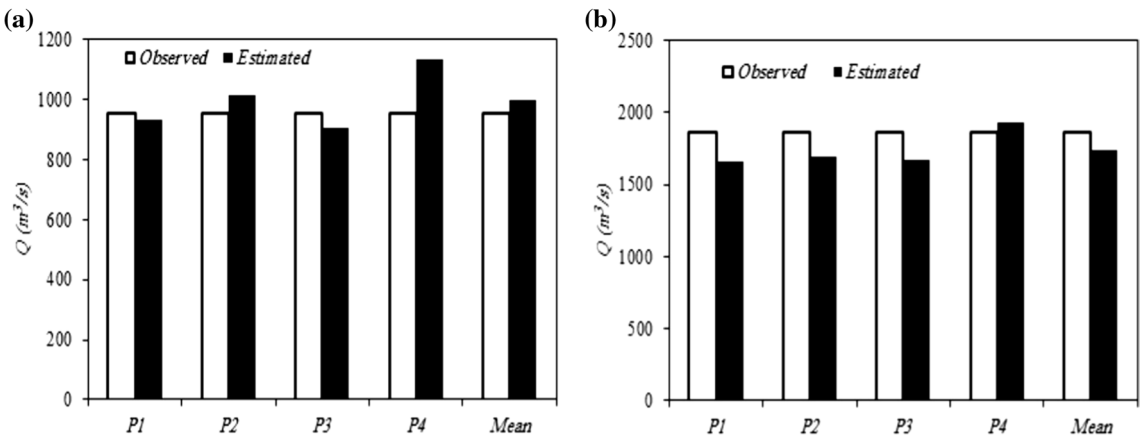

Fig. 8 Comparison between observed and estimated discharges at different water levels: **a** $H = 4.05$ m and **b** $H = 6.07$ m

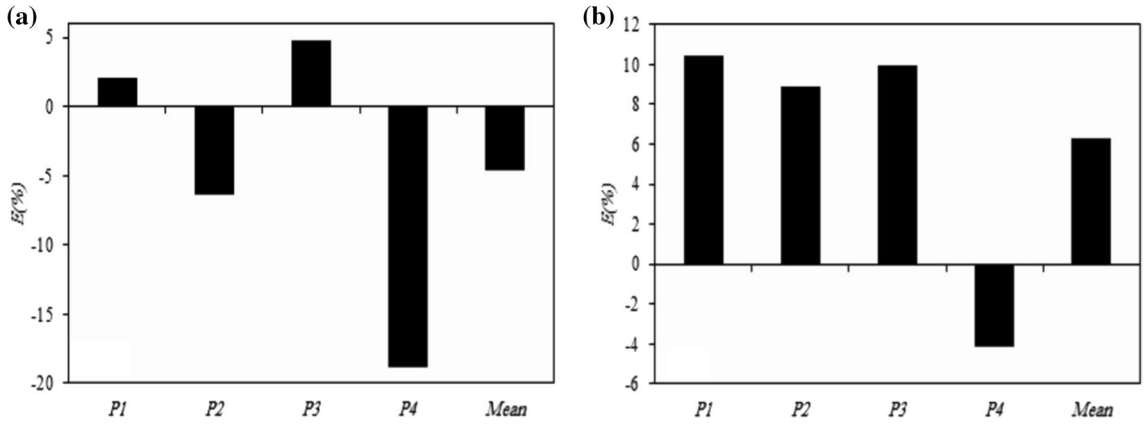

Fig. 9 Errors in discharge estimation by the SPM at two different water depths: **a** $H=4.05$ m and **b** $H=6.07$ m

levels to facilitate Eq. (12). Figure 10 shows the dimensionless values of these parameters up to the maximum level of $H_{max}=8.5$ m. The maximum values of A_{max}, P_{max}, $(P_t)_{max,}$ and $(U_{SPM})_{max}$ are 1566.25 m^2, 233.79 m, 463.88 m, and 72.96, respectively. Manning roughness coefficient distribution on the cross section is quasi-uniform, and its value is about 0.018.

Its value in Eq. (12) has no effect due to uniform roughness distribution. If the roughness distribution in the bed is heterogeneous, the equivalent roughness at each water level should be calculated using the weighted average method. As can be seen, the curve related to the parameters P and P_t has fractures in the floodplains due to sudden changes in the width of the water surface.

Figure 11 shows the stage–discharge curve estimated by the proposed method according to the estimated discharge data. In this method, the estimated stage–discharge curve passes through the point if the observed flow is used as the reference flow. However, it should be noted that the reference flow rate included at these levels is the same flow obtained from the SPM Method (SPM) and velocity. For example, in Fig. 11d, the curve does not exceed the corresponding flow rate of 6.07 m. The actual discharge is the basis for constructing the stage–discharge curve, not the estimated discharge from the SPM Method. This approach can reduce the accuracy of the estimated stage–discharge as the accuracy of the referenced discharge in this method is essential. Nonetheless, the main goal is the applicability and integration of surface velocity measurement and stage–discharge curve estimation.

For a more accurate analysis of the error value of the proposed method, two statistical parameters of mean absolute percentage error (MAPE), which was presented in Eq. 13, and normalized root squares deviation (NRMSE), have been used:

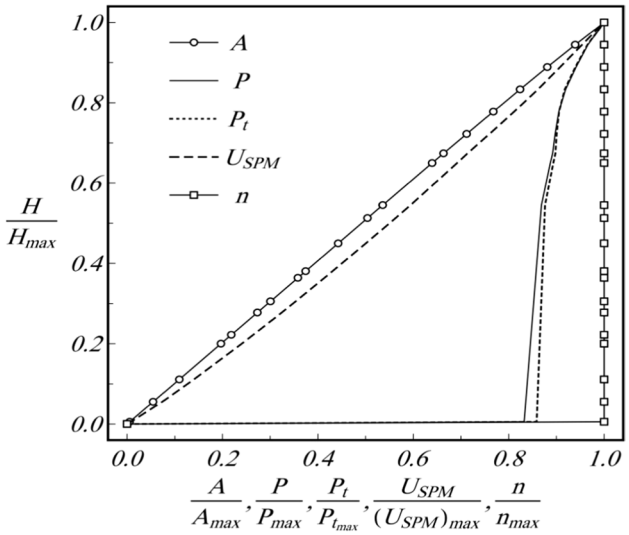

Fig. 10 Changes in parameters A, P, $P_{t,}$ and U_{SPM} in the Mollasani section

$$\mathrm{NRMSE}=\frac{\sqrt{\frac{1}{N}\sum_{i=1}^{N}\left(Q_{r,i}-Q_{e,i}\right)^2}}{\left(Q_r\right)_{\max}-\left(Q_r\right)_{\min}}. \tag{15}$$

The results obtained from Eqs. (13) and (15) are shown in Fig. 12. for all levels. As can be seen, the maximum value of MAPE is 9.6%, and the minimum value of this parameter is 4.05%. Also, the maximum and minimum NRMSE values are 0.122 and 0.034, respectively. Also, the results show that the mean values of MAPE and NRMSE are about 5.7% and 0.059, respectively. It should be noted that the accuracy of the observed point, which is considered a reference point, is critical.

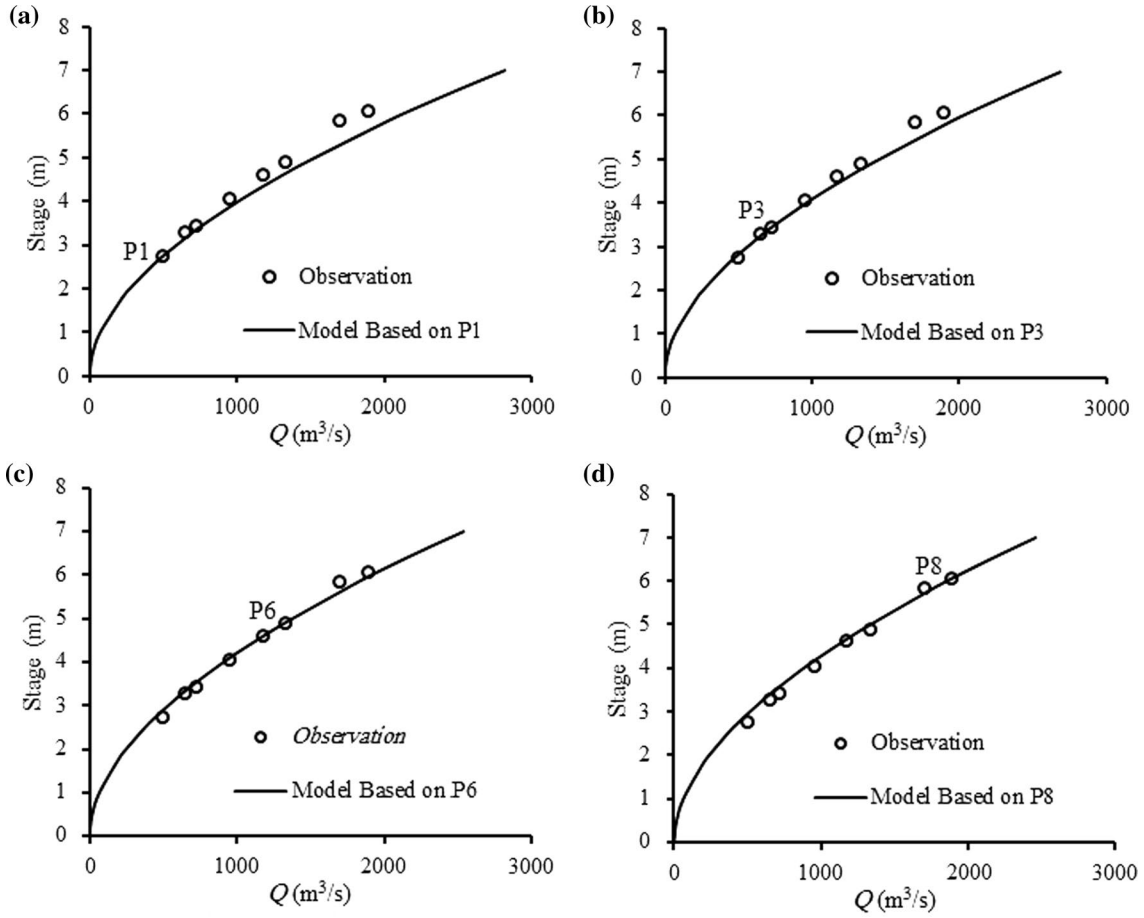

Fig. 11 Rating curves estimated in the Mollasani cross section based on different reference points

Discussion

One of the basic challenges is determining the discharge and rating curve during floods and managing the flood hazards in rivers without hydrometric stations. With the development process of advanced satellite sensors that provide more accurate spatial and digital information, the way to access remote flood data has been presented to researchers.

The present method can calculate discharge and stage–discharge using only a single point of velocity measurement at a river section. The only required inputs to the current model are solely the geometrical shape of the river extracted from Sentinel-1/2 and a single point of velocity measurement. Therefore, the paper's primary goal is to study the applicability and integration of surface velocity measurement and stage–discharge rating curve estimation.

At first, discharge was estimated based on each observed velocity measurement at P1, P2, P3, and P4 at two water levels, $H = 4.05$ and 6.07 m (Fig. 4). Based on all observed

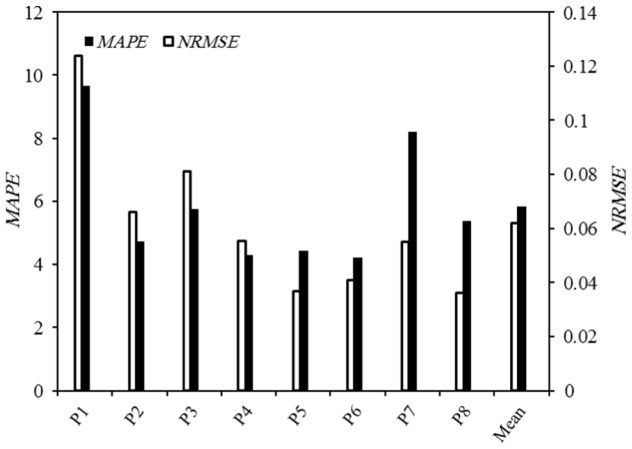

Fig. 12 Changes in MAPE and NRMSE values in estimating the stage–discharge curve in the Mollasani cross section

points, the maximum average discharge NPE and MAPE are limited to about 6.3% and 8.4. The estimated discharge is affected by the location of the surface velocity measuring locations across the water surface. Generally, there is a minor error when the point selected to measure the surface velocity is near the middle of the channel (Not necessarily at the thalweg line) and where water is still flowing in the main channel. Then, the stage–discharge rating curve is estimated by the proposed method according to the estimated discharge data from the previous step. The maximum value of MAPE and NRMSE is about 10% and 0.034, respectively. The proposed method obtains lower error values and a more accurate estimated flow rate and the stage–discharge curve when more points are used (Farnoush and Maghrebi 2021).

This method can be used instead of the conventional methods proposed to determine the mean velocity in a vertical profile by 80–90% of the water surface velocity (Genç et al. 2015). However, the conventional methods cannot consider the effect of geometry on the estimation of mean velocity. Also, the exact determination of a suitable coefficient to convert surface velocity to mean velocity is challenging and uncertain.

This method can be a suitable way to use remote sensing products. Sentinel 1/2 images were used in this study. However, images of other satellites such as Landsat (Al-Khudhairy et al. 2002), MODIS (Smith and Pavelsky 2008), and altimetry (Coe and Birkett 2004) can be used to extract cross-sectional geometric information and hydraulic parameters. In addition, *AirSAT* images can be used to estimate river surface velocity (Bjerklie et al. 2005).

Fundamental parameters in river discharge (Q) are depth (d), velocity(u), and width (w), and it can be considered as $Q = w \cdot d \cdot u$ where $w = aQ^b$,$d = eQ^f$ and $u = kQ^m$. With the experiences gained in the previous two decades, d, u, and w can be measured from space or airborne instruments. The present study is an approach to applying these parameters using Isovel pattern in the river section and can improve the estimation accuracy.

Conclusions

Discharge and rating curve estimation in natural rivers with irregular cross-sectional shapes, especially in ungauged rivers, are necessary and always complex for understanding and predicting many hydrologists and river engineering-related issues. In this type of cross section, using the single-point velocity measurement method (SPM), it is possible to obtain a proper estimate using minimum measurement data to simplify discharge estimation or corresponding water level prediction.

In this study, using two sets of measured surface velocity data at two different water levels at three points with different transverse positions in the river width and a point at the middle of the river width at 0.8 of depth, the discharge was estimated at the Mollasani station on the Karun the longest permanent river in Iran. Estimated discharges were used to evaluate the proposed method's efficiency and compare it with measured discharge values, which showed that an average error was not exceeding 8.36%. Estimating the stage–discharge curve using the method introduced by Maghrebi et al. (2017) is acceptable accuracy, has inherent simplicity, and does not require calibration. The results show that MAPE and NRMSE are about 5.7% and 0.059, respectively.

The main characteristic of the present study is that the hydrometric cost in ungauged rivers can be reduced drastically by using this method. The proposed model provides a satisfactory agreement compared to the observed data. Because there are fewer measurement data requirements, this methodology can be applied to natural rivers in deprived areas.

As mentioned in the explanation of the SPM section, based on the velocity distribution pattern in the cross section, the normalized velocity of a point is known at any position. Therefore, by knowing the ratio of the velocity of a point to the average velocity at the same position, the average velocity is calculated, and then flow rate is extracted. These calculations are presented in Tables 4 and 5. In this article, the extraction of geometric characteristics of the cross section was obtained using SAR images. On the other hand, by using RADAR and LIDAR images, it is possible to obtain the altimetry measurement information of the current section. Therefore, this article has tried to show the SPM theory method in a section of the Karun River in Iran based on the surface velocity measurement data in discharge estimation and the stage–discharge relationship. In addition, studies have also been conducted to use remote tools such as drones and RADAR altimetry to measure surface velocity. Therefore it can be proven that complete remote methods can be considered effective in discharge evaluation. Additionally, the extraction of the stage–discharge relationship in rivers based on the initial approximation is possible.

Availability of data and materials Data and material are available upon request to the corresponding author.

Declarations

Conflict of interest The authors declare that they have no known competing financial interests or personal relationships that could have appeared to influence the work reported in this paper.

References

Al-Khudhairy D, Leemhuis C, Hoffmann V, Shepherd IM, Calaon R (2002) Monitoring wetland ditch water levels using Landsat TM

and ground-based measurements. Photogramm Eng Remote Sens 68(8):809–818
Bjerklie DM, Moller D, Smith LC, Dingman SL (2005) Estimating discharge in rivers using remotely sensed hydraulic information. J Hydrol 309(1):191–209. https://doi.org/10.1016/j.jhydrol.2004.11.022
Boothroyd RJ, Williams RD, Hoey TB, Barrett B, Prasojo OA (2021) Applications of google earth engine in fluvial geomorphology for detecting river channel change. Wiley Interdiscip Rev: Water 8(1):e21496
Cavallo C, Nicolina PM, Gargiulo M, Palau-Salvador G, Vezza P, Ruello G (2021a) Continuous Monitoring of the flooding dynamics in the albuferawetland (Spain) by Landsat-8 and Sentinel-2 datasets. Remote Sens 2021(13):3525. https://doi.org/10.3390/rs13173525
Cavallo C, Nones M, Nicolina Papa M, Gargiulo M, Ruello G, (2021b) Monitoring the morphological evolution of a reach of the Italian Po River using multispectral satellite imagery and stage data. Geocarto International, Taylor & Francis Onlinehttps://doi.org/10.1080/10106049.2021.2002431
Chen C-L (1991) Unified theory on power laws for flow resistance. J Hydraul Eng 117(3):371–389. https://doi.org/10.1061/(ASCE)0733-9429(1991)117:3(371)
Coe MT, Birkett CM, (2004) Calculation of river discharge and prediction of lake height from satellite radar altimetry: Example for the Lake Chad Basin. Water Resour Res, 40(10), https://doi.org/10.1029/2003WR002543
Farnoush H, Maghrebi MF (2021) Application of surface velocimetry in estimating rating curves in compound channels. Flow Meas Instrum 82:402–409. https://doi.org/10.1016/j.flowmeasinst,2021.102049
Genç O, Ardıçlıoğlu M, Ağıralioğlu N (2015) Calculation of mean velocity and discharge using water surface velocity in small streams. Flow Meas Instrum 41:115–120
Gilvear DJ, Bryant R (2016) Analysis of remotely sensed data for fluvial geomorphology and river science. In: Kondolf M, Piegay H (eds) Tools in fluvial geomorphology. Wiley, Chichester, England, pp 103–132
Gleason C, Smith L, Lee J (2014) Retrieval of river discharge solely from satellite imagery and at-many-stations hydraulic geometry: sensitivity to river form and optimisation parameters. AGU Water Resour Res 50(12):9604–9619
Jiang H, Feng M, Zhu Y, Lu N, Huang J, Xiao T (2014) An automated method for extracting rivers and lakes from Landsat imagery. Remote Sens 6(6):5067–5089
Maghrebi MF (2006) Application of the single-point measurement in discharge estimation. Adv Water Resour 29(10):1504–1514. https://doi.org/10.1016/j.advwatres.2005.11.007
Maghrebi MF, Ahmadi A (2017) Stage-discharge prediction in natural rivers using an innovative approach. J Hydrol 545:172–181
Maghrebi MF, Ball JE (2006) New method for estimation of discharge. J Hydraul Eng 132(10):1044–1051. https://doi.org/10.1061/(ASCE)0733-9429(2006)132:10(1044),1044-1051
Maghrebi MF, Kavousizadeh A, Maghrebi RF, Ahmadi A (2017) Stage–discharge estimation in straight compound channels using isovel contours. Hydrol Process 31:3859–3870. https://doi.org/10.1002/hyp.11299
Maghrebi MF (2003) Discharge estimation in flumes using a new technique for the production of isovel contours, In: Proceeding Int. Conf. Civ. Environ. Eng. ICCEE: pp. 147–156
Matgen P, Schumann G, Henry JB, Hoffmann L, Pfister L (2007) Integration of SAR-derived river inundation areas, high-precision topographic data and a river flow model toward near real-time flood management. Int J Appl Earth Obs Geoinf 9(3):247–263
McFeeters SK (1996) The use of the Normalized Difference Water Index (NDWI) in the delineation of open water features. Int J Remote Sens 17:1425–1432
Paris A, Paiva R, Silva J, Moreira M, Calmant S, Garambois P, Collischonn W, Bonnet M, Seyler F (2016) Stage-discharge rating curves based on satellite altimetry and modeled discharge in the Amazon Basin. Water Resour Res. https://doi.org/10.1002/2014WR016618
Schumann G, Bates PD, Horritt MS, Matgen P, Pappenberger F. (2009) Progress in integration of remote sensing–derived flood extent and stage data and hydraulic models. Rev Geophys, 47(4). https://doi.org/10.1029/2008RG000274.
Smith LC, Isacks B, Forster R, Bloom A, Preuss I (1995) Estimation of discharge from braided glacial rivers using ERS 1 synthetic aperture radar: first results. Water Resour Res 31(5):1325–1329
Smith LC, Isacks BL, Bloom AL, Murray AB (1996) Estimation of discharge from three braided rivers using synthetic aperture radar satellite imagery: Potential application to ungauged basins. Water Resour Res 32(7):2021–2034
Smith LC, Pavelsky TM (2008) Estimation of river discharge, propagation speed, and hydraulic geometry from space: Lena River, Siberia. Water Resour Res, 44(3) https://doi.org/10.1029/2007WR006133
Tarpanelli A, Brocca L, Lacava T, Melone F, Moramarco T, Faruolo M, Pergola N, Tramutoli V (2013) Toward the estimation of river discharge variations using MODIS data in ungauged basins. Remote Sens Environ 136:47–55. https://doi.org/10.1016/j.rse.2013.04.010
Tian H, Li W, Wu M, Huang N, Li G, Li X, Niu Z (2017) Dynamic Monitoring of the largest freshwater lake in china using a new-water index derived from high spatiotemporal resolution sentinel-1A data. Remote Sens 9(6):521. https://doi.org/10.3390/rs9060521
Xu H (2006) Modification of normalised difference water index (NDWI) to enhance open water features in remotely sensed imagery. Int J Remote Sens 27(14):3025–3033
Xu K, Zhang J, Watanabe M, Sun C (2004) Estimating river discharge from very high-resolution satellite data: a case study in the Yangtze RiverChina. Hydrol Process 18(10):1927–1939. https://doi.org/10.1002/hyp.1458
Yen BC (2002) Open channel flow resistance. J Hydraul Eng 128(1):20–39. https://doi.org/10.1061/(ASCE)0733-9429(2002)128:1(20)